Indian Journal of Pure & Applied Physics
Vol. 57, June 2019, pp. 411-421

Spectroscopic characterization and natural bond orbital analysis of 2-(trifluoromethyl) phenylacetonitrile based on DFT calculations

M Padmavathy[a] & S Seshadri[b]*

[a]Department of Physics, Shrimati Indira Gandhi College, Trichy 620 002, India

[b]PG & Research Department of Physics, Urumu Dhanalakshmi College, Trichy 620 002, India

Received 31 August 2018; accepted 01 March 2019

The experimental Fourier transform infrared (FT-IR) and Fourier transform Raman (FT-Raman) spectra of 2-(trifluoromethyl)phenylacetonitrile (2TFMP) have been recorded in the spectral region 4000–400 cm^{-1} and 3500–100 cm^{-1}, respectively. Also the title molecule has been characterized by ^{13}C NMR and ^{1}H NMR spectroscopes. The geometry optimization and frequency calculations have been performed at B3LYP/6-311+G (d,p) level. A detailed interpretation of FT-IR and FT-Raman spectra aided by the potential energy distributions (PEDs) for the calculated frequencies has been reported. Results of this study showed that there is a good correlation between the experimental and computational results. The HOMO-LUMO energy gap explains the charge transfer interactions in the molecule. NBO (natural bond orbital) computations have been utilized to evaluate the stabilities which occur from charge delocalization and inter-molecular interactions have been studied using DFT calculations.

Keywords: FT-IR, FT-Raman, NMR, PED, NBO

1 Introduction

Phenylacetonitrile (a synonym of benzyl cyanide) and its derivatives are widely utilized in chemical and pharmaceutical industries. Chemical manufacturers currently synthesize phenylacetonitrile using cyanide, which was shown to be highly toxic to animals and may cause serious environmental pollution. Phenylacetonitrile contains molecules with ordered structure and is stabilized by dipole-dipole interactions, whereas alcohols are self-associated through the hydrogen bonding of their hydroxyl groups, creating multimers of different degrees. Alcohols are used as hydraulic fluids, in medications for animals, in manufacturing of perfumes, flavors and dyestuffs, paint removers, as defrosting and as an antiseptic agent. Phenylacetonitrile is used in organic synthesis of dyes, perfumes, pesticides, pharmaceuticals, especially penicillin precursors. Recently, substantial research work has been reported on the excess properties of acetonitrile+alkanols[1], acrylonitrile+alkanols[2,3] and benzonirile+alkanols[4], while that on phenylacetonitrile+alkanol is relatively rare.

Literature survey reveals that no detailed B3LYP with 6-311+G (d,p) basis set of FT-IR, FT-Raman and NMR (^{13}C and ^{1}H) chemical shifts calculation of 2TFMP have been reported so far. It is, therefore thought worth to make this theoretical and experimental vibrational spectroscopic research based on optimized molecular structure to give the correct assignment of fundamental bands in the experimentally observed FT-IR and FT-Raman spectra. In this study, molecular geometry and vibrational frequencies are calculated using hybrid density functional method. This method predicts relatively accurate molecular structure and vibrational spectra with moderate computational effort. Natural bond orbital analysis, molecular orbital's and NMR spectrum were analyzed by B3LYP method with 6-311+G (d,p) basis set. Specific scale factors were also used and employed in the predicted frequencies.

2 Experimental Details

The fine solid sample of 2-(trifluoromethyl) phenylacetonitrile (2TFMP) is purchased from Sigma-Aldrich chemicals, USA and it was used as such without any further purification. The FT-IR spectrum of the compound has been recorded using Perkin-Elimer 180 spectrometer in the range of 4000–400 cm^{-1}. The spectral resolution is ±2 cm^{-1}. The FT-Raman spectrum of the compound was also recorded in same instrument with FRA 106 Raman module

*Corresponding author (E-mail: kavinkarthick2017@gmail.com)

equipped with Nd:YAG laser source operating in the region 3500–100 cm^{-1} at 1064 nm line width with 200 Mw powers. ^{13}C and ^{1}H NMR spectra were taken in $CDCl_3$ solutions and all signals were referenced to TMS on a BRUKER TPX-400 FT-NMR spectrometer.

3 Computational Details

The entire calculations were performed at DFT/B3LYP level with 6-311+G (d,p) basis set using Gaussian 09W[5] program. B3LYP represents Becke's three parameter hybrid functional method[6] with Lee-Yang-Parr correlation functional (LYP)[4,7] is the best predicting results for molecular geometry and vibrational wavenumbers for moderately larger molecule. In order to fit the theoretical wavenumbers to the experimental, the scaling factors have been introduced by least square optimization method. The transformation of force field, subsequent normal coordinate analysis and calculation of the potential energy distribution (PED) were done on a PC with the MOLVIB program (Version 7.0-G77) written by Sundius[8]. The highest occupied molecular orbital (HOMO) and lowest unoccupied molecular orbital (LUMO) analysis of 2TFMP have been calculated by the same level of theory.

The natural bonding orbital (NBO) calculation[9] were performed using NBO 3.1 program as implemented in Gaussian 09W[5] package at B3LYP method in order to understand various second order interactions between the another subsystem, which is a measure of the intramolecular delocalization or hyper-conjugation. NMR Chemical shielding anisotropy parameters are calculated using B3LYP level with same basis set.

3.1 Prediction of Raman intensities

The Raman activities (S_i) calculated with the Gaussian[5] 09W program are converted to relative Raman intensities (I_i) using the following relationship derived from the basic theory of Raman scattering[10]:

$$I_i = \frac{f(v_0 - v_i)^4 s_i}{v_i\left[1 - \exp\left(\frac{-hcv_i}{k_b T}\right)\right]} \quad \ldots (1)$$

where v_0 is the exciting frequency (in cm^{-1} units), v_i is the vibrational wavenumbers of the i^{th} normal mode, h, c, and k_b are universal constants, T is the temperature and f is the suitably chosen common scaling factor for all the peak intensities.

4 Results and Discussion

4.1 Structural analysis

The molecular structure of the 2TFMP belongs to C1 point group symmetry. The optimized molecular structure of title molecule is shown in Fig. 1. Table 1 compares the calculated bond lengths, bond angles and dihedral angles. The title molecule contains one methylene group, one nitrile group and a trifluoromethyl group connected with benzene ring.

4.2 Vibrational spectral analysis

The vibrational spectra of 2TFMP have not been described in detail in the literature. Therefore, we focused on title compound, the observed and simulated FT-IR and FT-Raman spectra of the title compound are shown in Figs 2 and 3, respectively. The title molecule consists of 19 atoms, which undergoes 51 normal modes of vibrations. Of the 51 normal modes of vibrations, 35 modes of vibrations are in-plane and remaining 16 are out-of-plane. The in-plane of the molecule is represented as A′ and out-of-plane as A″. Thus the 42 normal modes of vibrations are distributed as Γ_{Vib} = 35 A′+ 16 A″. In agreement with C1 symmetry all the 51 fundamental vibrations are active in both IR absorption and Raman scattering. The harmonic vibrational frequencies are calculated for title molecule at DFT (B3LYP) level using the triple split valence basis set along with the diffuse and polarization functions, 6-311+G (d,p) observed FT-IR and FT-Raman frequencies for various modes of vibrations have been presented in Table 2.

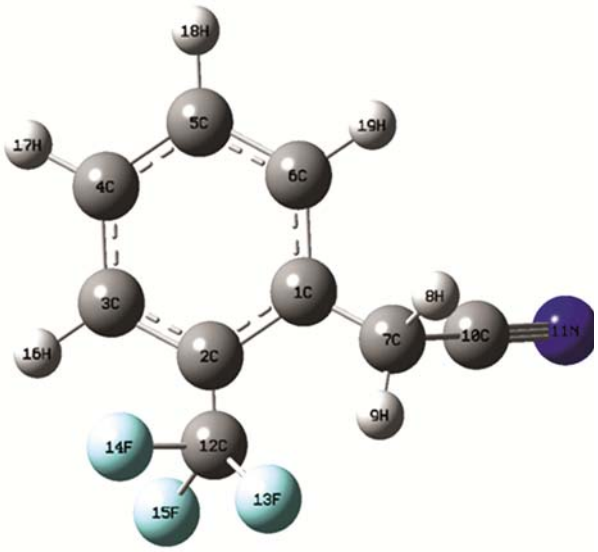

Fig.1 — Molecular structure of 2TFMP atoms are numbering.

Table 1 — Optimized geometrical parameters of 2TFMP calculated by B3LYP/6-311+G (d,p) level of theory.

Bond length	Values (Å)	Bond angle	Values (º)	Dihedral angles	Values (º)
C1–C2	1.416	C2–C1–C6	121.114	C6–C1–C2–C3	–0.001
C1–C6	1.407	C2–C1–C7	119.853	C6–C1–C2–C12	–180.004
C1–C7	1.434	C6–C1–C7	119.031	C7–C1–C2–C3	–180.005
C2–C3	1.398	C1–C2–C3	117.508	C7–C1–C2–C12	–0.009
C2–C12	1.508	C1–C2–C12	121.151	C2–C1–C6–C5	0.584
C3–C4	1.397	C3–C2–C12	121.339	C2–C1–C6–H19	179.999
C3–H16	1.086	C2–C3–C4	121.536	C7–C1–C6–C5	180.00
C4–C5	1.397	C2–C3–H16	118.868	C1–C7–C10–N11	179.235
C4–H17	1.086	C4–C3–H16	119.545	C1–C2–C3–C4	0.002
C5–C6	1.393	C3–C4–C5	120.293	C1–C2–C3–H16	180.002
C5–H18	1.085	C3–C4–H17	119.665	C12–C2–C3–C4	180.009
C6–H19	1.085	C5–C4–H17	120.040	C12–C2–C3–H16	0.009
C7–H8	1.087	C1–C7–H8	120.345	C1–C7–C10–H8	180.231
C7–H9	1.088	C1–C7–H9	120.346	C1–C7–C10–H9	180.243
C10–N11	1.164	C4–C5–C6	119.510	C1–C2–C12–F13	–180.073
C12–F13	1.092	C1–C6–H19	120.515	C1–C2–C12–F14	–59.505
C12–F14	1.095	C6–C5–H18	119.974	C1–C2–C12–F15	59.490
C12–F15	1.095	C1–C6–C5	120.302	C3–C2–C12–F13	–0.008
		C1–C6–H19	119.274	C3–C2–C12–F14	120.493
		C5–C6–H19	120.695	C3–C2–C12–F15	–120.510
		C2–C12–F13	110.885	C2–C3–C4–C5	–0.001
		C2–C12–F14	111.304	C2–C3–C4–H17	180.036
		C2–C12–F15	111.303	H16–C3–C4–C5	179.993
		F13–C12–F14	108.198	C3–C4–C5–C6	–0.001
		F13–C12–F15	108.199	C3–C4–C5–H18	180.045
		F14–C12–F15	106.785	H17–C4–C5–H18	–180.001
		C7–C10–N11	126.023	C4–C5–C6–C1	0.001
				C4–C5–C6–H19	180.001
				H18–C5–C6–C1	180.003
				H18–C5–C6–H19	0.543

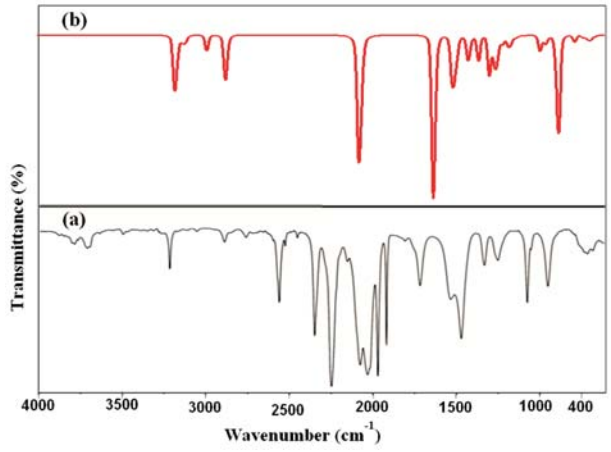

Fig. 2 — Observed (a) and calculated (b) FT-IR spectra of 2TFMP.

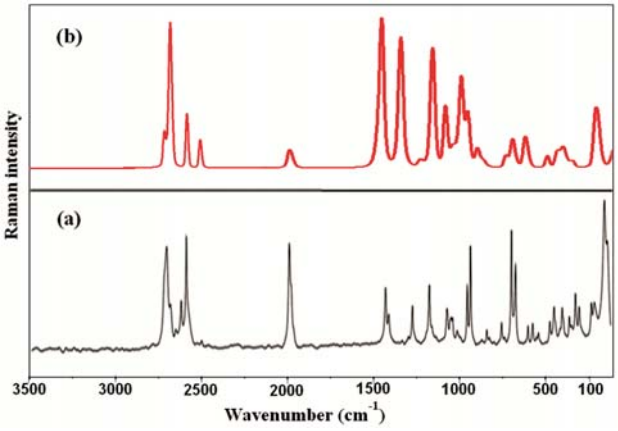

Fig. 3 — Observed (a) and calculated (b) FT-Raman spectra of 2TFMP.

In order to fit the theoretical wave numbers to that of experimental, the scaling factor is introduced by a least square optimization of the computed values to the experimental data. Vibrational frequencies are scaled by 0.962. By combining the results of Gauss view program along with literature values, the

Table 2 — Vibrational assignments of fundamental frequencies are obtained for 2TFMP along with IR intensities (Kmmol^{-1}), Raman intensities (q$\tilde{o}^4$amu^{-1}), depolarization ratios for plane (P) and unpolarized (U), reduced masses (amu), force constants (mDyne/A) using B3LYP/6-311G+(d,p) level of theory.

Modes	Experimental frequencies (cm^{-1})		Calculated frequencies (cm^{-1})		IR intensity	Raman intensity	Reduced mass	Force constant	Depolarization		[a]Vibrational assignments (PED > 10%)
	FT-IR	FT-Raman	Unscaled	Scaled					(P)	(U)	
1			3353	3251	7.64	7.65	1.08	33.66	0.27	0.42	νCH(98)
2	3250(m)		3230	3156	90.48	45.12	4.34	25.11	0.39	0.56	νCH(98)
3			3192	3106	4.81	64.29	1.11	6.24	0.10	0.18	νCH(97)
4			3103	2945	1.29	56.06	56.06	6.15	0.62	0.77	νCH(96)
5			3076	2896	1.94	24.72	124.72	6.12	0.54	0.71	CH_2asym (97)
6	2900(vw)		3029	2832	5.26	63.77	63.77	6.05	0.63	0.77	CH_2sym (87)
7	2756(vw)	2725(vs)	2942	2803	12.30	100.52	1.21	6.17	0.29	0.45	νCN(64)+βCH(35)
8	1850(vs)	2000(vs)	1827	1795	57.36	88.97	1.11	5.23	0.52	0.68	νCC(74)+βCC(27)
9	1725(m)		1625	1592	248.14	72.76	1.53	3.71	0.47	0.64	νCC(72)+βCN(29)
10	1540(vw)		1584	1532	104.47	25.89	3.35	4.96	0.52	0.69	νCC(71)+βCH(23)
11	1500(m)		1564	1504	22.67	63.43	2.94	4.25	0.33	0.50	CF_3asym(57)+βCC(37)
12	1460(m)		1474	1421	30.58	40.96	2.07	2.65	0.11	0.21	CF_3asym(53)+βCH(26)
13		1425(s)	1450	1402	65.78	15.64	1.59	1.98	0.51	0.67	νCC(75)+βCH(29)
14	1315(m)		1370	1325	39.49	17.19	1.33	1.47	0.74	0.85	νCC(64)+βCH(29)
15		1270(m)	1313	1285	17.66	32.05	1.93	1.95	0.15	0.26	νCC(61)+βCH(29)
16	1250(m)		1246	1184	30.16	77.88	1.52	1.39	0.50	0.67	CF_3sym(51)+βCH(34)
17			1208	1156	76.49	66.88	1.28	1.10	0.72	0.84	νCC(69)+βCH(21)
18		1150(m)	1169	1112	5.40	28.05	2.39	1.92	0.26	0.42	νCC(72)+βCH(27)
19			1136	1098	5.49	52.80	2.36	1.79	0.58	0.73	νCC(63)+βCH(31)
20	1100(s)		1115	1056	10.35	10.01	2.20	1.61	0.65	0.79	CH_2sciss(78)+βCH(18)
21			1082	1025	3.47	47.27	2.12	1.47	0.15	0.27	Rtrigd (37)+βCC(21)
22		1025(vw)	1054	985	0.14	5.67	1.32	0.86	0.72	0.84	βCH(53)+CF_3asym(18)
23	1000(s)		984	947	1.27	3.27	1.35	0.83	0.66	0.79	Rasymd(32)+βCC(17)
24			943	912	10.23	11.55	6.02	3.15	0.11	0.19	Rsymd(36)+βCC (19)
25	915(m)		916	872	1.65	4.14	1.29	0.64	0.24	0.38	βCH(58)+CF_3asym(16)
26			906	845	12.29	69.38	7.24	3.51	0.29	0.45	βCH(56)+CF_3sym(13)
27		850(vs)	843	823	22.34	59.22	4.93	2.06	0.40	0.57	βCH(53)+CF_3asym(18)
28			830	813	64.38	5.18	1.16	0.47	0.75	0.85	CH_2rock(70)+ βCC(23)
29			836	795	3.4.59	11.91	10.95	3.50	0.74	0.84	CF_3ipb(34)+Rsymd(25)
30			785	765	1.41	16.46	8.17	2.26	0.69	0.82	CF_3opb(32)+Rtrigd(21)
31		760(w)	752	732	6.73	58.39	9.82	2.54	0.48	0.65	γCH(37)+γCH(18)
32			725	702	6.77	12.05	6.41	1.52	0.73	0.85	γCH(37)+γCH(21)
33			692	674	1.11	13.41	4.81	1.06	0.19	0.33	γCH(37)+γCC(21)
34		650(vs)	635	601	20.19	43.08	6.82	0.98	0.60	0.75	CF_3sb(34)+βCN(22)
35		625(s)	575	542	9.84	75.91	5.93	0.79	0.21	0.35	γCH(37)+γCC(21)
36		580(w)	552	521	10.39	12.86	6.22	0.61	0.71	0.83	CF_3ipr(22)+tRsymd(18)
37			527	503	11.94	55.66	6.24	0.56	0.12	0.22	βCC(42)+βCC(21)
38			518	495	11.44	29.17	4.85	0.38	0.36	0.53	βCC(43)+βCH(25)
39			505	473	1.01	33.83	5.25	0.31	0.73	0.84	βCC(40)+βCCO(18)
40		490(vw)	491	455	23.12	57.17	11.17	0.34	0.67	0.80	γCC(38)+ γCN(23)
41			484	436	6.96	2.46	7.63	0.15	0.68	0.81	γCC(35)+tRasymd(23)
42			452	411	1.27	12.88	11.72	0.04	0.69	0.82	CF_3opr(22)+tRsymd(16)
13			427	392	0.57	3.46	6.92	0.08	0.70	0.83	CH_2wagg (48)+νCN (13)
44		410(m)	405	376	3.41	56.56	13.06	0.62	0.28	0.73	βCN(35)+βCH(24)

(*contd.*)

Table 2 — Vibrational assignments of fundamental frequencies are obtained for 2TFMP along with IR intensities (Kmmol^{-1}), Raman intensities (ɖ^{4}amu^{-1}), depolarization ratios for plane (P) and unpolarized (U), reduced masses (amu), force constants (mDyne/A) using B3LYP/6-311G+(d,p) level of theory. (*contd.*)

Modes	Experimental frequencies (cm^{-1})		Calculated frequencies (cm^{-1})		IR intensity	Raman intensity	Reduced mass	Force constant	Depolarization		[a]Vibrational assignments (PED > 10%)
	FT-IR	FT-Raman	Unscaled	Scaled					(P)	(U)	
45		390(w)	382	357	14.33	49.23	10.47	0.83	0.47	0.64	tRtrigd(29)+γCC(14)
46			343	338	4.51	36.81	5.83	0.90	0.0	0.12	CH_2twist(31)+γCN(CH_2) (17)
47			342	312	7.11	87.60	6.43	3.04	0.39	0.56	γCC(32)+tRsymd(13)
48			225	216	19.67	46.08	3.09	1.67	0.31	0.48	γCN(35)+tRasymd(23)
49		180(m)	198	167	56.09	25.37	1.06	2.36	0.73	0.84	tRasymd(27)+γCN(13)
50		160(vw)	163	143	9.95	29.82	1.05	3.41	0.18	0.31	tRsymd(24)+γCC(16)
51			108	98	1.51	13.06	1.08	4.39	0.74	0.85	tCF3(29)+ γCH(14)

Experimental relative intensities are abbreviated as follows: vs-very strong, s-strong, m-medium, w-weak, w-very weak. asym-asymmetric stretching, sym-symmetric stretching, β-in-plane bending, γ-out-of-plane bending, sciss-scissoring, rock-rocking, wagg-wagging, twist-twisting, R-ring, trigd-trigonal deformation, symd-symmetric deformation, asymd-asymmetric deformation, ipb-in-plane bending, opb-out-of-plane bending, sb-symmetric bending, ipr-in-plane rock, opr-out-of-plane rock, t-torsion.[a]Scaling factor: 0.962forB3LYP/6-311+G(d,p).

vibrational frequency assignments are made here with a high degree of accuracy. After scaling the deviation from the experiments is found to be less than 10 cm^{-1}, with a few exceptions.

4.2.1 C–H vibrations

The carbon and hydrogen atoms are bonded by single covalent bonds in 2TFMP. This gives rise to four C–H stretching; four C–H in-plane bending vibrations and four C–H out-of-plane bending vibrations. The hetero aromatic structure shows the presence of C–H stretching vibration in the region 3100–3000 cm^{-1} which is the characteristic region for the ready identification of C–H stretching vibration[11]. In this region, the bands are not affected appreciably by the nature of substituents. The C–H stretching mode usually appears with strong Raman intensity and is highly polarized. In the FT-IR spectrum of title molecule, the medium band at 3250 cm^{-1} is assigned to C–H stretching vibration of hetro cyclic group. The theoretically computed wavenumber by B3LYP method falls at 3251, 3156, 3106 and 2945 cm^{-1} which is assigned to C–H stretching vibrations. The PED corresponding to this vibration is a pure mode and contributing of 98%.

The C–H in-plane bending frequencies appear in the range 1000–1300 cm^{-1} and are very useful for characterization purpose[12]. For our title molecule, the C–H in-plane bending vibrations appear as a medium band in FT-IR spectrum at 915 cm^{-1} and 1025, 850 cm^{-1} as a very weak and strong band in FT-Raman spectrum shows good agreement with calculated frequencies. The PED confirms these vibrations of mixed mode as it is evident from Table 2 almost contributing 59%. The C–H out-of-plane[13] bending vibrations are strongly coupled vibrations and occur in the region 1000–750 cm^{-1}. The aromatic C–H out-of-plane bending vibrations are assigned as weak band in FT-Raman spectrum at 760 cm^{-1} well correlated with theoretical values.

4.2.2 C–C vibrations

The aromatic C–C stretching vibration occurs in the region[12] 1589–1301 cm^{-1}. In the present work, the wavenumbers observed at 1850, 1725, 1540 and 1315 cm^{-1} in the FT-IR spectrum, 2000, 1425, 1270 and 1150 cm^{-1} in the FT-Raman spectrum are in good agreement with theoretically calculated values. In 2TFMP, the CCC in-plane bending vibrations are observed at 1000 cm^{-1} in FT-IR spectrum. These assignments are in good agreement with the literature[14]. The CCC out-of-plane bending bands are appeared in the expected range. This shows that the theoretically computed values may be mixing other vibrations.

4.2.3 CH_2 vibrations

For the assignments of CH_2 group frequencies, basically six fundamentals can be associated to each CH_2 group namely, CH_2 symmetric stretching; CH_2 asymmetric stretching; CH_2 scissoring; and CH_2 rocking that belongs to in-plane vibrations and two out-of-plane vibrations such as CH_2 wagging and CH_2 twisting modes, which are expected to be depolarized[15]. The asymmetric CH_2 stretching vibrations are generally observed above 3000 cm^{-1},

while the symmetric stretch[16] will appear between 3000 and 2900 cm^{-1}. The CH_2 asymmetric stretching vibration is missing in the observed FT-IR and FT-Raman spectrum and symmetric stretching vibrations are observed in FT-IR 2900 (m) cm^{-1} of title compound. This band is calculated at 2832 cm^{-1}. The in-plane and out-of-plane bending vibrations are observed within the characteristics range.

4.2.4 CF_3 Vibrations

Usually symmetric and antisymmetric CF_3 stretching vibrations are in the ranges 1290–1235cm^{-1} and 1226–1200 cm^{-1}, respectively[17, 18]. Therefore the band observed at 1500 and 1460 cm^{-1} in FT-IR spectrum are assigned to asymmetric stretching vibrations. CF_3 symmetric frequency is observed at 1250 in FT-IR spectrum, the same calculated at 2832 cm^{-1} for title compound. CF_3 deformations[19] usually occur in regions 690–631 cm^{-1}, 640–580 cm^{-1} and 570–510 cm^{-1}. Accordingly CF_3 symmetric bending is identified at 580 cm^{-1} in FT-Raman spectrum.

4.2.5 C≡N vibrations

For the aromatic compound which bears a C≡N group attached to the ring, a band of very strong intensity has been observed in the region 2220–2240 cm^{-1} and it is being attributed to C≡N stretching vibration[20]. Futher, the n-π conjugation between the cyano nitrogen lone electron pair and the phenyl ring is strong in the ground state. The very weak band obtained at 2756 cm^{-1} in FT-IR and 2725 cm^{-1} in FT-Raman spectra are assigned to C≡N stretching vibration for 2TFMP. The in-plane and out-of-plane bending modes of C≡N group are strongly coupled with CCC bending modes. They are due to the out-of-plane aromatic ring deformation with in-plane deformation of the C≡N vibration and in-plane bending of the aromatic ring with the C–C≡N bending. In this study, the C≡N in-plane vibration is found at 410 cm^{-1} in FT-Raman and the out-of-plane C≡N bending mode is calculated with null IR intensity and very weak or almost null Raman activity, in accordance with the no-detection of this mode in the experimental spectra. The calculated band 216 cm^{-1} is assigned to the out-of-plane deformation of C≡N vibration for the title molecule.

4.3 NBO analysis

NBO analysis provides the most accurate possible 'natural Lewis structure' and all orbital details are mathematically chosen to include the highest possible percentage of the electron density. A useful aspect of the NBO method is that it gives information about interactions in both filled and virtual orbital spaces that could enhance the analysis of intra- and inter-molecular interactions.

The second-order Fock matrix was carried out to evaluate the donor–acceptor interactions in the NBO analysis[21]. The interactions result is a loss of occupancy from the localized NBO of the idealized Lewis structure into an empty non-Lewis orbital. For each donor (i) and acceptor (j), the stabilization energy $E^{(2)}$ associated with the delocalization i→j is estimated as:

$$E^{(2)} = -n_\sigma \frac{\langle \sigma | F | \sigma \rangle^2}{\varepsilon_{\sigma^*} - \varepsilon_\sigma} = -n_\sigma \frac{F_{ij}^2}{\Delta E} \quad \ldots (2)$$

where $\langle \sigma | F | \sigma \rangle^2$ or F_{ij}^2 is the Fock matrix element between the *i* and *j* NBO orbital, ε_{σ^*} and ε_σ are the energies of σ and σ* NBO's and n_σ is the population of the donor σ orbital.

NBO analysis has been carried out to explain the charge transfer or delocalization of charge due to the intra-molecular interaction among bonds and also provides a convenient basis for investigating charge transfer or conjugative interaction in molecular systems. Some electron donor orbital, acceptor orbital and the interacting stabilization energy resulting from the second order micro disturbance theory is reported[22,23]. The larger the stabilization energy value, the more intensive is the interaction between electron donors and electron acceptors, i.e., the more donating tendency from electron donors to electron acceptors and the greater the extent of conjugation of the whole system. Delocalization of electron density between occupied Lewis-type (bond or lone pair) NBO orbitals and formally unoccupied (anti-bond or Rydberg) non-Lewis NBO orbitals correspond to a stabilizing donor-acceptor interaction. NBO calculation is performed using Gaussian 09W[5] package program at the B3LYP level in order to understand various second order interactions between the filled orbital of one subsystem and vacant orbital of another subsystem, which is a measure of the delocalization or hyper conjugation. The corresponding results have been given in Tables 3 and 4.

Table 3 — Selected NBO results showing formation of Lewis and non-Lewis orbital for 2TFMP calculated by B3LYP/6-311+G(d,p) method.

Bond (A–B)	ED/energy (a.u)	ED_A (%)	ED_B (%)	NBO	S(%)	P(%)
BD(C1–C2)	1.970	50.86	49.14	0.713($sp^{1.72}$) C+0.701 ($sp^{1.92}$)C	36.80	63.17
					34.18	65.78
BD(C1–C6)	1.972	51.71	48.29	0.719($sp^{1.72}$) C+0.694 ($sp^{1.90}$)C	36.78	63.19
					34.52	65.44
BD(C1–C7)	1.983	50.00	50.00	0.707 ($sp^{2.78}$) C+0.707 ($sp^{0.91}$)C	26.43	73.52
					52.23	47.73
BD(C2–C3)	1.974	51.08	48.92	0.715 ($s^{1.82}$) C+0.699 ($sp^{1.87}$)	35.39	64.57
					34.82	65.14
BD(C7–H9)	1.982	51.92	48.08	0.721 ($sp^{2.29}$) C+0.693 ($sp^{3.00}$)H	30.40	69.57
					24.98	74.97
BD(C3–C4)	1.979	50.22	49.78	0.708 ($sp^{1.85}$) C+0.705 ($sp^{1.85}$)C	35.12	64.84
					35.12	64.81
BD(C4–H17)	1.980	62.73	37.27	0.7920 ($sp^{2.33}$) C+0.711 ($sp^{0.01}$)H	30.04	69.92
					99.95	0.05
BD(C4–C5)	1.980	49.99	50.01	0.707 ($sp^{1.84}$) C+0.707 ($sp^{1.85}$)C	35.15	64.81
					35.13	64.82
BD(C5–H18)	1.982	62.76	37.24	0.792 ($sp^{2.36}$) C+0.612 ($sp^{0.10}$)H	29.71	70.25
					99.94	0.06
BD(C5–C6)	1.977	49.57	50.43	0.704 ($sp^{1.87}$) C+0.710 ($sp^{1.80}$)C	34.87	65.08
					35.67	64.29
BD(C2–C12)	1.659	51.54	48.46	0.717 ($sp^{1.00}$) C+0.696 ($sp^{1.00}$)C	0.00	99.96
					0.00	99.96
BD(C6–H19)	1.981	62.89	37.11	0.793 ($sp^{2.34}$) C+0.609($sp^{1.00}$)	29.97	70.00
					99.95	0.05
BD(C7–H8)	1.980	63.25	36.75	0.795 ($sp^{2.35}$) C+0.606 ($sp^{2.00}$)H	29.80	70.17
					99.95	0.05
BD(C10–N11)	1.996	42.04	57.96	0.648 ($sp^{1.07}$) C+0.761 ($sp^{1.11}$)N	48.20	51.78
					47.25	52.34
BD(C12–F13)	1.987	62.36	37.64	0.789 ($sp^{3.00}$) C+0.6135 ($sp^{2.00}$)F	24.96	0.05
					99.95	75.25
BD(C12–F14)	1.977	62.76	37.24	0.792 ($sp^{3.05}$) C+0.610($sp^{0.00}$)F	24.70	75.25
					99.95	0.05
BD(C12–F15)	1.985	62.87	37.13	0.792 ($sp^{2.95}$)C+0.609 ($sp^{0.00}$)F	25.31	74.65
					99.95	0.05

The intra-molecular interactions are observed as increase in electron density (ED) in (C–N) anti-bonding orbital that weakens the respective bonds. The electron density of conjugated bond of substitution (1.996 a.u) clearly demonstrates strong delocalization. The occupancy of π bonds is lesser than σ bonds which lead more delocalization.

The intra-molecular hyperconjugative interaction of distribute to σ electrons of σ*(C5–C6) to the anti σ*(C1–C2) bond in the ring leads to stabilization of some part of the ring as evident from Table 4. The intra-molecular hyper-conjugative interaction of the σ*(C5–C6) to the anti σ

*(C1–C2) bond in the ring leads to stabilization of 22.16 and 23.87 kcal/mol.

4.4 Frontier molecular orbital analysis

The total energy, energy gap and dipole moment have effect on the stability of a molecule. The optimization is used in order to investigate the energetic behavior and dipole moment of title compound in gas phase and with two different solvents. The frontier molecular orbitals (FMOs) play an important role in the optical and electric properties, as well as in quantum chemistry and UV-Vis spectra[24]. The HOMO is the orbital that primarily acts as an electron donor and the LUMO is the orbital that largely acts as the electron acceptor and the gap between HOMO and LUMO characterizes the molecular chemical stability, chemical reactivity, optical polarizability and chemical hardness and

Table 4 — Second order perturbation theory analysis of Fock matrix on NBO basis for 2TFMP using B3LYP method with 6-311+G(d,p) basis set.

Donor NBO (i)	Acceptor NBO (j)	$E^{(2)a}$ kcal/mol	$E(i) - E(j)^b$ (a.u)	$F(i,j)^c$ (a.u)
BD (C1–C2)	BD*(C1–C6)	3.98	1.28	0.064
BD (C1–C2)	BD*(C1–C7)	1.25	1.09	0.033
BD (C1–C2)	BD*(C2–C3)	2.81	1.29	0.054
BD (C1–C2)	BD*(C2–C12)	1.26	1.10	0.033
BD (C1–C2)	BD*(C3–H16)	2.05	1.17	0.054
BD (C1–C2)	BD*(C6–H19)	2.11	1.17	0.033
BD (C1–C2)	BD*(C10–N11)	3.70	1.66	0.044
BD (C1–C2)	BD*(C3–C4)	16.66	0.29	0.070
BD (C1–C2)	BD*(C5–C6)	22.16	0.29	0.021
BD (C1–C2)	BD*(C7–H8)	11.95	0.38	0.062
BD (C1–C2)	BD*(C7–H9)	1.86	0.74	0.065
BD (C1–C6)	BD*(C1–C2)	4.30	1.29	0.021
BD (C1–C6)	BD*(C1–C7)	1.25	1.09	0.036
BD (C1–C6)	BD*(C2–C12)	3.33	1.09	0.067
BD (C1–C6)	BD*(C5–H18)	2.11	1.17	0.054
BD (C1–C6)	BD*(C6–H19)	1.07	1.16	0.047
BD (C1–C6)	BD*(C7–C10)	3.56	1.66	0.044
BD (C1–C6)	BD*(C10–N11)	0.96	0.83	0.032
BD (C1–C7)	BD*(C1–C2)	1.17	1.25	0.069
BD (C1–C7)	BD*(C1–C6)	0.97	1.23	0.025
BD (C1–C7)	BD*(C2–C3)	3.07	1.24	0.034
BD (C1–C7)	BD*(C5–C6)	2.45	1.24	0.031
BD (C1–C7)	BD*(C7–C10)	2.85	1.61	0.055
BD (C2–C3)	BD*(C1–C2)	3.51	1.28	0.049
BD (C2–C3)	BD*(C1–C7)	3.81	1.08	0.061
BD (C2–C3)	BD*(C3–C4)	2.38	1.28	0.057
BD (C2–C3)	BD*(C3–H16)	0.93	1.15	0.032
BD (C2–C3)	BD*(C4–H17)	2.24	1.16	0.049
BD (C2–C12)	BD*(C1–C2)	1.49	1.18	0.029
BD (C2–C12)	BD*(C1–C6)	3.20	1.16	0.046
BD (C2–C12)	BD*(C2–C3)	1.43	1.17	0.037
BD (C2–C12)	BD*(C3–C4)	2.60	1.17	0.054
BD (C3–C4)	BD*(C2–C3)	2.64	1.28	0.037
BD (C3–C4)	BD*(C2–C12)	3.54	1.08	0.049
BD (C3–C4)	BD*(C3–H16)	1.05	1.15	0.052
BD (C3–C4)	BD*(C4–C5)	2.14	1.27	0.055
BD (C3–C4)	BD*(C4–H17)	0.91	1.15	0.031
BD (C3–C4)	BD*(C5–H18)	2.41	1.15	0.047
BD (C3–C4)	BD*(C1–C2)	23.87	0.28	0.074
BD (C3–C4)	BD*(C5–C6)	18.58	0.28	0.065
BD (C3–H16)	BD*(C1–C2)	4.71	1.10	0.064
BD (C3–H16)	BD*(C2–C3)	1.11	1.10	0.031
BD (C3–H16)	BD*(C3–C4)	0.79	1.09	0.026
BD (C3–H16)	BD*(C4–C5)	3.57	1.09	0.056
BD (C4–C5)	BD*(C3–C4)	2.19	1.27	0.047
BD (C4–C5)	BD*(C3–H16)	2.48	1.15	0.048
BD (C4–C5)	BD*(C4–H17)	0.92	1.15	0.029
BD (C4–C5)	BD*(C5–C6)	2.17	1.27	0.047

(*contd.*)

Table 4 — Second order perturbation theory analysis of Fock matrix on NBO basis for 2TFMP using B3LYP method with 6-311+G(d,p) basis set.

Donor NBO (i)	Acceptor NBO (j)	$E^{(2)a}$ kcal/mol	$E(i) - E(j)^b$ (a.u)	$F(i,j)^c$ (a.u)
BD (C4–C5)	BD*(C5–H18)	0.97	1.15	0.030
BD (C4–C5)	BD*(C6–H19)	2.37	1.15	0.047
BD (C4–H17)	BD*(C2–C3)	3.52	1.10	0.056
BD (C4–H17)	BD*(C3–C4)	0.69	1.09	0.024
BD (C4–H17)	BD*(C4–C5)	0.72	1.09	0.025
BD (C4–H17)	BD*(C5–C6)	3.70	1.09	0.057
BD (C5–C6)	BD*(C1–C6)	2.68	1.27	0.052
BD (C5–C6)	BD*(C1–C7)	4.06	1.07	0.059
BD (C5–C6)	BD*(C4–C5)	2.15	1.27	0.047
BD (C5–C6)	BD*(C4–H17)	2.38	1.15	0.047
BD (C5–C6)	BD*(C5–H18)	0.90	1.15	0.029
BD (C5–C6)	BD*(C6–H19)	1.00	1.15	0.030
BD (C5–C6)	BD*(C3–C4)	18.01	0.28	0.064
BD (C5–C6)	BD*(C1–C2)	21.31	0.28	0.069
BD(C5–H18)	BD*(C3–C4)	3.80	1.09	0.057
BD(C5–H18)	BD*(C1–C6)	3.67	1.09	0.057
BD(C5–H18)	BD*(C3–C4)	0.76	1.09	0.026
BD(C5–H18)	BD*(C4–C5)	0.78	1.09	0.026
BD(C6–H19)	BD*(C1–C2)	4.15	1.10	0.060
BD(C6–H19)	BD*(C1–C6)	0.80	1.09	0.026
BD(C6–H19)	BD*(C4–C5)	3.70	1.09	0.057
BD(C6–H19)	BD*(C5–C6)	0.85	1.09	0.027
BD(C10–N11)	BD*(C1–C7)	3.11	1.43	0.060
BD(C10–N11)	BD*(C1–C6)	1.82	0.90	0.036
BD(C10–N11)	BD*(C1–C2)	4.69	0.36	0.041
BD(C12–F13)	BD*(C1–C2)	3.32	1.09	0.054
BD(C12–F13)	BD*(C2–C3)	0.94	0.54	0.022
BD(C12–F14)	BD*(C1–C2)	3.92	0.53	0.045
BD(C12–F14)	BD*(C2–C3)	0.55	1.08	0.022
BD(C12–F15)	BD*(C1–C2)	0.94	0.53	0.022
BD(C12–F15)	BD*(C2–C3)	3.09	1.08	0.052
BD(C7–H8)	BD*(C1–C7)	0.89	1.08	0.028
BD(C7–H9)	BD*(C1–C7)	3.73	1.08	0.059

[a]$E^{(2)}$mean energy of hyper conjugative interactions (stabilization energy).

[b]Energy difference between donor and acceptor i and j NBO orbitals.

[c]F(i,j) is the Fock matrix element between i and j NBO orbital.

softness of a molecule[25]. The energy gap between the HOMO and the LUMO is a critical parameter in determining molecular electrical transport properties because it is a measure of electron conductivity.

Surfaces for the frontier orbitals were drawn to understand the bonding scheme of present molecule. The two molecular orbitals are examined for title molecule: the highest occupied MOs and the lowest unoccupied MOs are represented as HOMO and LUMO, respectively. A 3D diagram of HOMO and LUMO orbitals are illustrated using B3LYP/6-311+G (d,p) basis set for 2TFMP.

According to the Fig. 4, In the case of HOMO, charges are distributed almost over all the atoms of molecule. The red colour represents the negative charges or the electron distribution and the green colour represents the positive charges or the deprival of electrons. While comparing HOMO and LUMO the negative and positive charges are not equally distributed. HOMO is localized on the whole molecule which spitted up into many rings, which

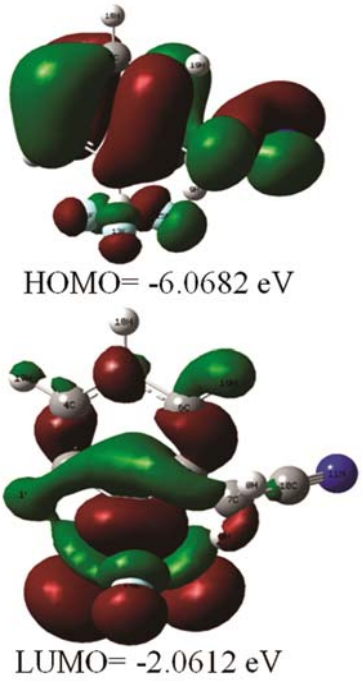

Fig. 4 — HUMO and LUMO plot of 2TFMP.

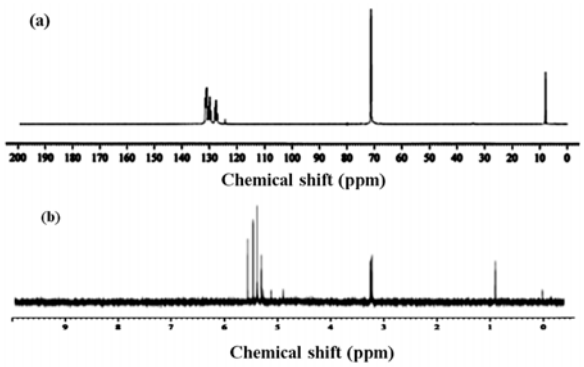

Fig. 5 — Experimental (a) ^{13}C NMR and (b) ^{1}H NMR spectra of 2TFMP.

shows that the almost all the rings are bound at methyl group which divided into two C–H bonds each one carries positive and negative charges. But in LUMO is localized on all the carbon atoms of 2TFMP, which shows that all the carbon atoms have neutral charges. Since fluorine group vibrations are generally referred to electron donating substituent in the hydrocarbon compounds. The energy gap is found to be -4.0072 eV for title compound. The HOMO-LUMO transition implies an electron density transfer of methylene to nitrile group region.

4.5 NMR spectral analysis

The ^{13}C and ^{1}H NMR chemical shifts are calculated within gauge independent atomic orbital (GIAO) method using B3LYP/6-311+G (d,p) level. A comparison of the experimental and theoretical spectra can be very useful in making correct assignments and understanding the basic chemical shift molecular structure relationship. The experimental ^{13}C and ^{1}H NMR spectra of the title compound are given in Fig. 5((a) ^{13}C and (b) ^{1}H)). In Table 5, the experimental and the theoretical ^{13}C and ^{1}H isotropic chemical shifts in ppm for the title compound are presented. The ^{13}C chemical shift values for all calculations have the range from 157.294 to 73.612 ppm at B3LYP/6-311+G(d,p) level of theory in average for 2TFMP. Downfield and upfield chemical shift values observed at 133 and 70 ppm of carbons C3 and C10 are due to electron donating effectof nitrile group. The carbon atoms C2, C5 and C6 are significantly observed in the upfield with chemical shift values 122, 127 and 131 ppm, respectively, which reveals that the influences of the electronegative nitrile and trifluoromethyl group atoms are negligibly small and their signal are observed in the normal range.

The ^{1}H chemical shift values for all calculations from 9.53 to 3.41 ppm at B3LYP/6-311+G(d,p) method in the average for 2TFMP molecule. As can be seen from Table 5, theoretical ^{13}C and ^{1}H chemical shift results of the title compound are generally closer to the corresponding experimental chemical shift data except for C2 atom. The small shifts can be explained as a consequence of the change in the molecular environment.

Table 5 — The experimental and calculated ^{13}C and ^{1}H NMR isotropic chemical shifts (ppm) of 2TFMP by B3LYP/6-311+G(d,p) method.

Atoms	Calculated	Experimental
C1	152.127	-
C2	118.283	122
C3	139.471	133
C4	157.294	-
C5	128.364	127
C6	130.524	131
C7	87.231	-
C10	73.612	70
C12	81.821	-
H8	9.53	-
H9	8.13	-
H16	5.82	5.6
H17	6.43	5.8
H18	5.44	5.4
H19	3.41	3.3

5 Conclusions

The FT-IR, FT-Raman and NMR (^{13}C and ^{1}H) spectra of the compound 2TFMP have been recorded and analyzed. The detailed interpretations of the vibrational spectra have been carried out. The observed wave numbers are found to be in good agreement with the calculated values. The optimized geometrical parameters (bond lengths, bond angles and dihedral angles) are theoretically determined by B3LYP/6-311+G(d,p) level of theory. The ^{13}C and ^{1}H NMR chemical shifts results seemed to be in a good agreement with experimental data. The HOMO-LUMO gap, which is consequence of the enhanced charge transfer between the donor and the acceptor group. Using NBO analysis the stability of the molecule arising from hyper-conjugative interaction and charge delocalization has been analyzed.

References

1 Nikam P S, Shirsat L N & Hasan M, *J Chem Eng Data*, 43 (1998) 732.
2 Sandhu J S & Singh A, *J Chem Thermodyn*, 24 (1992) 81.
3 Aralguppi M I, Jadar C V & Aminabhavi T M, *J Chem Eng Data*, 44 (1999) 446.
4 Nikam P S, Jagdale B S, Sawant A B & Hasan M, *J Chem Eng Data*, 45 (2000) 214.
5 Frisch M J et al., Gaussian Inc., Gaussian 09 Revision, A11.4, Pittsburgh, PA, 2008.
6 Becke A D, *J Chem Phys,* 98 (1993) 5648.
7 Lee C, Yang W & Parr R C, *Phys Rev B,* 37 (1998) 785.
8 Sundius T, MOLVIB: *A program for Harmonic Force Field Calculations*, QCPE Program No. 807, 2002.
9 Glendening E D, Reed A E, Carpenter J E & Weinhold F. NBO Version 3.1. TCI. University of Wisconsin, Madison, 1998.
10 Chocholousova J, Vladimir Spirko V & Hobza P, *Chem Phys*, 6 (2004) 37.
11 Balachandran V & Parimala K, *J Mol Struct,* 1007 (2012) 136.
12 Varsanyi G, *Assignments for Vibrational Spectra of Seven Hundred Benzene Derivatives*, (Academic Kiaclo: Budapet), 1973.
13 Sebastian S, Sundaraganesan N, Karthikeiyan B & Srinivasan V, *Spectrochim Acta*, 78A (2011) 590.
14 Peesole R L, Shield L D & Mcwillam I C, *Modern Methods of Chemical Analysis*, (Wiley: New York), 1976.
15 Durig J R, Little T S, Gounev T K, Gardner J K & Sullivan J F, *J Mol Struct*, 375 (1996) 83.
16 Litivinov G, *Proceedings of the XIII International Conference on Raman Spectroscopy*, (Wurzburg: Germany), 1992.
17 Silverstein R M, Clayton Basseler G & Morrill T C, *Spectrometric identification of Organic Compounds*, (John Wiley and Sons: New York), 1991.
18 Balachandran V & Parimala K, *Spectrochem Acta*, 102A (2013) 30.
19 Fernandez L.E, Ben Altabet A & Varetti E L, *J Mol Struct*, 5 (2002) 612.
20 Smith B, *Infrared Spectral Interpretation, A Systematic Approach*, (CRC Press: Washington), 1999.
21 Sajan D, Hubert Joe I & Jayakumar V S, *J Raman Spectrosc*, 37 (2006) 508.
22 Kolev T, *J Mol Struct*, 349 (1995) 381.
23 Saravanan S P, Sankar A & Parimala K, *J Mol Struct*, 1127 (2017) 784.
24 24 Dollish F R, Fateley W G & Bentley F F, *Characteristic Raman Frequencies of Organic Compounds*, (John Wiley and Sons: New York), 1997.
25 Szafran M, Komasa A & Adamska E B, *J Mol Struct (Theochem)*, 827 (2007) 101.
26 James C, Amal Raj A, Reghunathan R, Hubert Joe R & Jayakumar V S, *J Raman Spectrosc*, 37 (2006) 1381.
27 Fleming I, *Frontier Orbitals, Organic Chemical Reactions*, (Wiley: London), 1976.
28 Kosar B & Albayrak C, *Spectrochim Acta*, 78A (2011) 160.